Journal of the Mechanical Behavior of Biomedical Materials 74 (2017) 195–203

Contents lists available at ScienceDirect

Journal of the Mechanical Behavior of Biomedical Materials

journal homepage: www.elsevier.com/locate/jmbbm

Corrosion and tribocorrosion behavior of $Ti-TiB-TiN_x$ in-situ hybrid composite synthesized by reactive hot pressing

J.I. Silva[a], A.C. Alves[a], A.M. Pinto[a,b], F. Toptan[a,b,*]

[a] CMEMS-UMinho, Center for MicroElectroMechanical Systems, Universidade do Minho, Azurém, 4800-058 Guimarães, Portugal
[b] Universidade do Minho, Dept. Eng. Mecânica, Azurém, 4800-058 Guimarães, Portugal

ARTICLE INFO

Keywords:
Corrosion
In-situ composites
Titanium
Tribocorrosion

ABSTRACT

Ti and its alloys are attractive materials for variety of fields, including biomedical implants, however, the wear behavior is yet to be improved. In the present work, $Ti-TiB-TiN_x$ in-situ metal matrix composites were synthesized by reactive hot pressing using a Ti-BN powder blend. Corrosion behavior was investigated in 9 g/L NaCl solution at 37 °C by performing potentiodynamic polarization and electrochemical impedance spectroscopy. Tribocorrosion behavior was investigated using reciprocating tribometer, against an alumina ball, under 1 and 10 N normal load, 1 and 2 Hz frequency, in 9 g/L NaCl solution at 37 °C. Results suggested that TiB and TiN_x in-situ phases did not deteriorate the corrosion behavior of Ti but significantly improved the tribocorrosion behavior under 1 N.

1. Introduction

Owing to their properties such as high specific strength, long fatigue life, excellent corrosion resistance and biocompatibility, Ti and its alloys are attractive materials for various industrial and biomedical applications (Bolzoni et al., 2012; Li et al., 2013; Rautray et al., 2011). However, poor wear resistance is the bottleneck of Ti and its alloys. Biomedical implants suffer relative movements against bone in corrosive body fluids (i.e. tribocorrosion), resulting with the release of wear debris and metal ions, that can interact with local tissues leading to an adverse response, ultimately leading to implant failure (Bryant et al., 2014; Licausi et al., 2013). Hard coatings have extensively been studied in order to overcome the low wear or tribocorrosion resistance of Ti, however, low fracture toughness of ceramic layers is still a major concern (Mathew et al., 2009; Rahaman et al., 2007; Wood, 2007).

Metal matrix composites (MMCs), which have been successfully used in many industrial wear-resistant applications for many years, have been considered as an alternative to overcome the risks related to the low fracture toughness of ceramics (Rosso, 2006). Although it is very well known after several decades of experience that the addition of hard reinforcing phases result in a substantial improvement on wear resistance of a metallic material, wear behavior of MMCs depend on several materials-related factors, together with mechanical and physical factors. Thus, wear should always be considered as a system property, more than a material property (Chawla and Chawla, 2006; Sannino and Rack, 1995; Toptan and Rocha, 2015). Accordingly, while Archard's law which shows a correlation between the hardness and the wear resistance can be applicable for monolithic materials, it may not give efficient results for MMCs since particularly the properties of the matrix/reinforcement interface may govern the wear behavior (Sannino and Rack, 1995; Venkataraman and Sundararajan, 1996). If the physical contact or the bonding between the matrix and the reinforcement is not sufficient, some reinforcement particles may be pulled-out under sliding and may act as extra abrasives (third-body particles) which may result in catastrophic wear, thus may even result in worse wear resistance as compared to the unreinforced matrix metal (Doni et al., 2014; Mondal and Das, 2006; Toptan et al., 2013; Velhinho et al., 2004). On the other hand, in electrochemical point of view, discontinuities at the matrix/reinforcement interface or the reaction products between the matrix and the reinforcement can cause localized corrosion at the interface (Ribeiro et al., 2015; Toptan et al., 2016). Moreover, in the presence of the load-carrying hard ceramic phases, the electrochemical behavior of the composite under sliding can exhibit significant deviations from the classical behavior of the passive metals. For example, a recent study from some of the present authors on the tribocorrosion behavior of $Ti-B_4C$ composites (Toptan et al., 2016) showed that under static conditions composite samples presented localized corrosion on the pore sites located at the agglomerated reinforcement particle zones. However, composite samples presented lower tendency to corrosion and lower corrosion kinetics under sliding, mainly due to the load carrying effect given by the B_4C particles, together with the contribution of decreased localized corrosion after

* Corresponding author at: CMEMS-UMinho, Center for MicroElectroMechanical Systems, Universidade do Minho, Azurém, 4800-058 Guimarães, Portugal.
E-mail address: ftoptan@dem.uminho.pt (F. Toptan).

http://dx.doi.org/10.1016/j.jmbbm.2017.05.041
Received 28 February 2017; Received in revised form 27 May 2017; Accepted 31 May 2017
Available online 08 June 2017

closure of the pores by the wear products.

Interface-related problems that are often observed on ex-situ composites can be eliminated by in-situ composites, where usually stronger interfaces are obtained (Aikin, 1997; Ranganath, 1997). In our previous work (Silva et al., 2016), as compared to the unreinforced Ti, Ti−TiB−TiN_x in-situ hybrid composite synthesized by reactive hot pressing exhibited nearly 4 times lower wear loss under dry sliding wear conditions, even relatively high contact pressures (0.89 GPa maximum Hertzian contact pressure for the unreinforced Ti) were applied. Although it can be considered as a candidate for several applications including biomedical ones where simultaneous action of corrosion and wear (i.e. tribocorrosion) takes place, to the best of our knowledge, there is no study available in the literature reporting the tribocorrosion behavior of this composite. Thus, the present study aims at studying the corrosion and tribocorrosion behavior of Ti−TiB−TiN_x in-situ hybrid composite.

2. Experimental procedure

Prior to processing, a powder mixture of the matrix metal (Ti) and the reactant (BN) was prepared with the Ti to BN weight ratio of 23:1, containing 35.5 and 1 μm average particle sizes of Ti and BN, respectively. Ti−TiB−TiN_x hybrid composite samples (10 mm in diameter and 4 mm in height) were synthesized by reactive hot pressing at 1100 °C during 30 min under 10^{-2} mbar vacuum and 40 MPa constant pressure. Unreinforced Ti samples were also processed under identical conditions to be used as control group. The details of the processing procedure is given elsewhere (Silva et al., 2016).

Sample surfaces were prepared for the corrosion and tribocorrosion tests by grinding down to 2400 mesh size SiC paper and polishing with colloidal silica suspension down to 0.04 μm. The surface roughness (R_a) after mirror finishing was measured using a non-contact profilometer (Veeco Dektak) as 0.09 ± 0.03 μm for the unreinforced Ti and 0.05 ± 0.02 μm for the composite. After surface preparation, samples were ultrasonically cleaned in propanol for 10 min and rinsed in distilled water during 5 min. Each sample was kept in desiccator for 24 h before starting each corrosion or tribocorrosion test.

Corrosion tests were performed in a three-electrode electrochemical cell (adapted from ASTM: G3-89) placed in a thermal bath to keep the electrolyte (180 mL of 9 g/L NaCl solution) at body temperature (37 ± 2 °C). A saturated calomel reference electrode (SCE), Pt counter electrode, and geometric exposed sample surface area of 0.38 cm^2 as working electrode were placed in the cell and connected to Gamry Potentiostat/Galvanostat/ZRA (model Referece-600). After stabilizing surfaces at open circuit potential (OCP), i.e. when ΔE was below 60 mV h^{-1}, EIS measurements were performed by scanning a range of frequencies from 100 kHz till 10 mHz with 10 points per frequency decade where the amplitude of the sinusoidal was set as 10 mV in order to guarantee linearity of the electrode response. Afterwards, the polarization scan was performed in anodic direction, starting at −0.9 V to 1 V with a scanning rate of 1 mV s^{-1}.

Tribocorrosion tests were performed in a ball-on-plate tribometer (CETR-UMT-2) with a reciprocating plate adapter having a thermal bath allowing to perform the experiments at body temperature (37 ± 2 °C). A triboelectrochemical cell containing 30 mL of 9 g/L NaCl solution was placed in the tribometer with the two electrode set-up using a SCE reference electrode, and samples having 0.79 cm^2 geometric exposed area as working electrode, connected to a Voltalab PGP201 potentiostat. The OCP was monitored before, during and after sliding where the sliding action against the counter material (10 mm diameter alumina ball, Ceratec) started after a stabilization period of 7200 s. Two different normal loads (1 and 10 N) were applied, corresponding to maximum Hertzian contact pressures of 0.41 and 0.89 GPa for the unreinforced Ti, respectively. On the lower load level, which is closer to biomedical implant applications, two different frequencies (1 and 2 Hz) were applied. Total stroke length and total sliding time were chosen as 3 mm and 1800 s, respectively, for all testing conditions. After sliding, the OCP values kept on being monitored during 1020 s in order to observe the repassivation behavior.

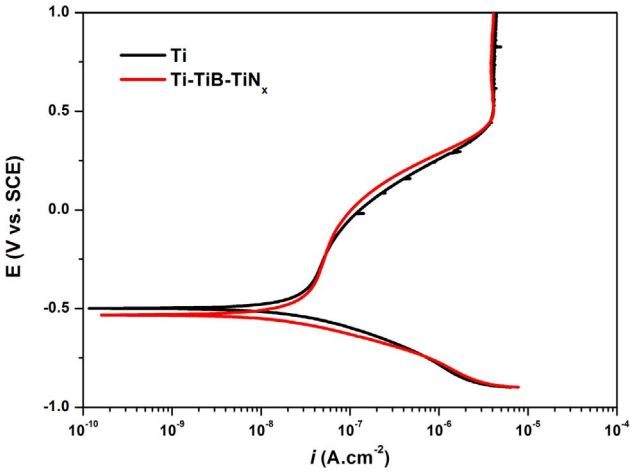

Fig. 1. Potentiodynamic polarization curves.

Table 1
i_{pass} and $E_{(i\ =\ 0)}$ values for Ti and Ti−TiB−TiN_x.

Sample	i_{pass} (×10^{-6}A.cm^{-2})	$E_{(i=0)}$ (mV)
Ti	4.34 ± 0.53	−489 ± 57
Ti−TiB−TiN_x	4.01 ± 0.63	−432 ± 122

Tested surfaces were ultrasonically cleaned following the procedure applied before the tests. Worn sample and counter material surfaces were analyzed by FEI Nova 200 field emission gun scanning electron microscope (FEG-SEM), equipped with EDAX energy dispersive X-ray spectroscopy (EDS). All worn surface images were taken as parallel to the sliding direction by using backscattered (BSE) and secondary electron (SE) detector signals. Total wear volume loss were calculated by considering five 2D profiles taken from each wear track using a non-contact profilometer (Veeco Dektak) and following the calculation procedure given elsewhere (Doni et al., 2013). All tests were triplicated for each group in order to have repeatability, and all results were given as the arithmetic mean ± standard deviation.

3. Results

Detailed structural and microstructural characterization of the Ti−TiB−TiN_x in-situ hybrid composite had previously been presented elsewhere (Silva et al., 2016), where SEM/EDS and XRD analysis had revealed that the structure is composed of Ti, TiB whiskers, and sub-stoichiometric TiN_x phases that led to a significant increase of hardness for the composite (736 ± 65 HV) as compared to the unreinforced Ti (316 ± 27 HV) (Silva et al., 2016).

Fig. 1 presents the potentiodynamic polarization curves of the unreinforced Ti and the composite samples and Table 1 gives the average passivation current density (i_{pass}) and corrosion potential ($E_{(i\ =\ 0)}$) values derived from the potantiodynamic polarization curves. In anodic domain, both materials presented a well-defined passivation plateau due to the formation of the passive oxide film. Since both materials presented very similar polarization behavior, together with similar $E_{(i\ =\ 0)}$ and i_{pass} values, it can be stated that the formation of TiB and TiN_x in-situ phases did not affect significantly the overall corrosion behavior of Ti.

Fig. 2 presents the EIS diagram in the form Nyquist and Bode. Nyquist diagram can be evaluated by comparing the diameters of the semi-circles where larger diameter indicates a better corrosion resistance (González and Mirza-Rosca, 1999). As can be observed in the Nyquist

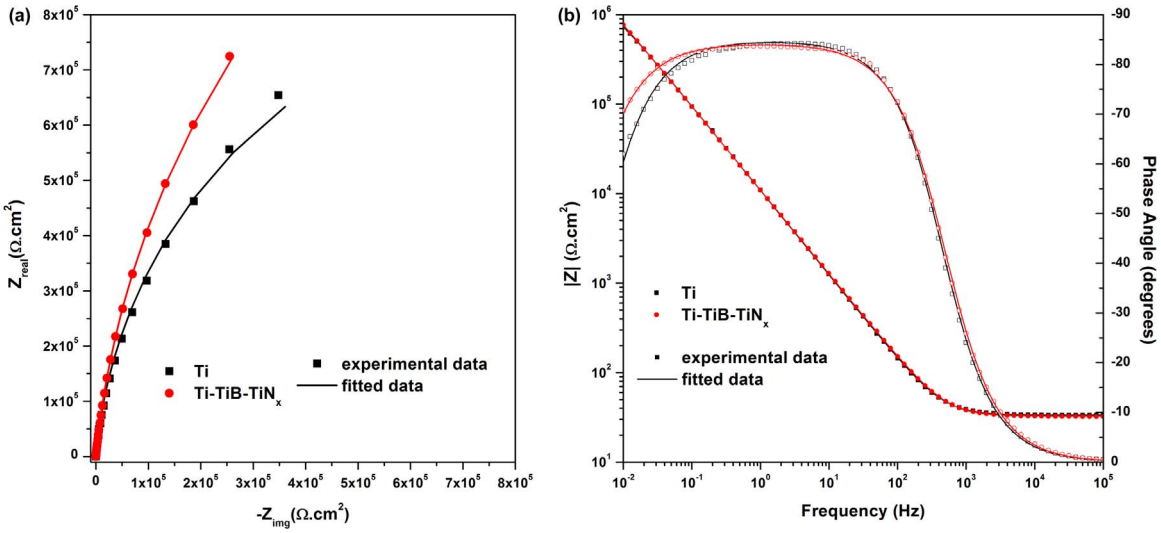

Fig. 2. (a) Nyquist and (b) Bode diagrams of experimental data and fitted curves.

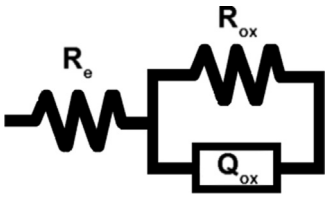

Fig. 3. Equivalent circuit used for fitting the experimental data.

Table 2
Equivalent circuit parameters obtained from EIS data for Ti and Ti − TiB − TiN_x.

Sample	R_{ox} ($\times 10^6$ Ω cm^2)	C_{ox} (μF cm^{-2})
Ti	1.40 ± 0.30	10.15 ± 0.54
Ti − TiB − TiN_x	2.62 ± 0.69	10.28 ± 1.67

diagram (Fig. 2a) the composite samples presented a slightly larger diameter of the semi-circle when compared to the Ti samples. The Bode diagram (Fig. 2b) shows constant values of |Z| in high frequency range (1000 Hz to 10 kHz) where the phase angle is near to 0° corresponding to the electrolyte resistance (González and Mirza-Rosca, 1999). As can be observed in the Bode diagram, in the low and middle frequency range, the phase angle values approached to −90° for both materials reflecting the typical capacitive behavior of a compact oxide film (Assis et al., 2006).

The impedance spectra were fitted to the electrical equivalent circuit (EEC) using Z-View software (version 2.9) by evaluating the quality of the fitting through their chi-square (χ^2) values. The EEC representing the native oxide film formed on surfaces of both Ti and Ti − TiB − TiN_x samples contains electrolyte resistance, R_e, native oxide film resistance (passive film), R_{ox}, and constant phase element (CPE), Q_{ox}, considering the non-ideal capacitance of the native oxide film (Fig. 3). CPE is defined as $Z_{CPE} = [Y_0(jw)^n]^{-1}$, where $-1 \leq n \leq 1$. When $n = -1$, $n = 0$ and $n = 1$, the CPE responses corresponds to those of an inductor, a resistor or a capacitor, respectively. When $n \approx 1$, a non-ideal capacitor may be described by CPE where the n value is being influenced by the roughness and heterogeneities on the surface (Figueira et al., 2009). All samples presented range of n values between 0.94 and 0.95, thus the proposed model describes adequately the behavior of the native oxide film in contact with NaCl, with chi-square below 1×10^{-4}.

Table 2 presents the EEC parameters obtained from EIS data for Ti and Ti − TiB − TiN_x. Q values were converted to C (capacitance) by using Eq. (1) derived from Brugg's equation (Orazem and Tribollet, 2008). C_{ox} values did not present any significant difference whereas slightly increased R_{ox} values were observed on the composite samples suggesting a slightly higher resistance for the passive layer formed on the composite surfaces.

$$C_{ox} = [Q_{ox} R_e^{(1-n)}]^{\frac{1}{n}} \quad (1)$$

The representative evolution of OCP before, during, and after sliding is given in Fig. 4, together with the evolution of coefficient of

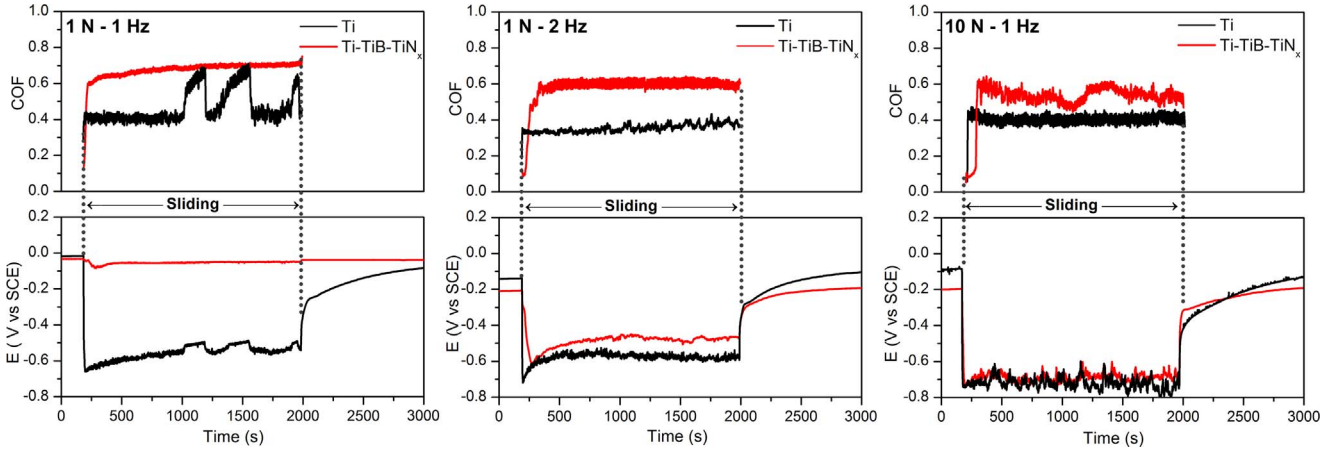

Fig. 4. Evolution of COF under sliding, together with evolution of OCP before, during and after sliding in 9 g/L NaCl solution.

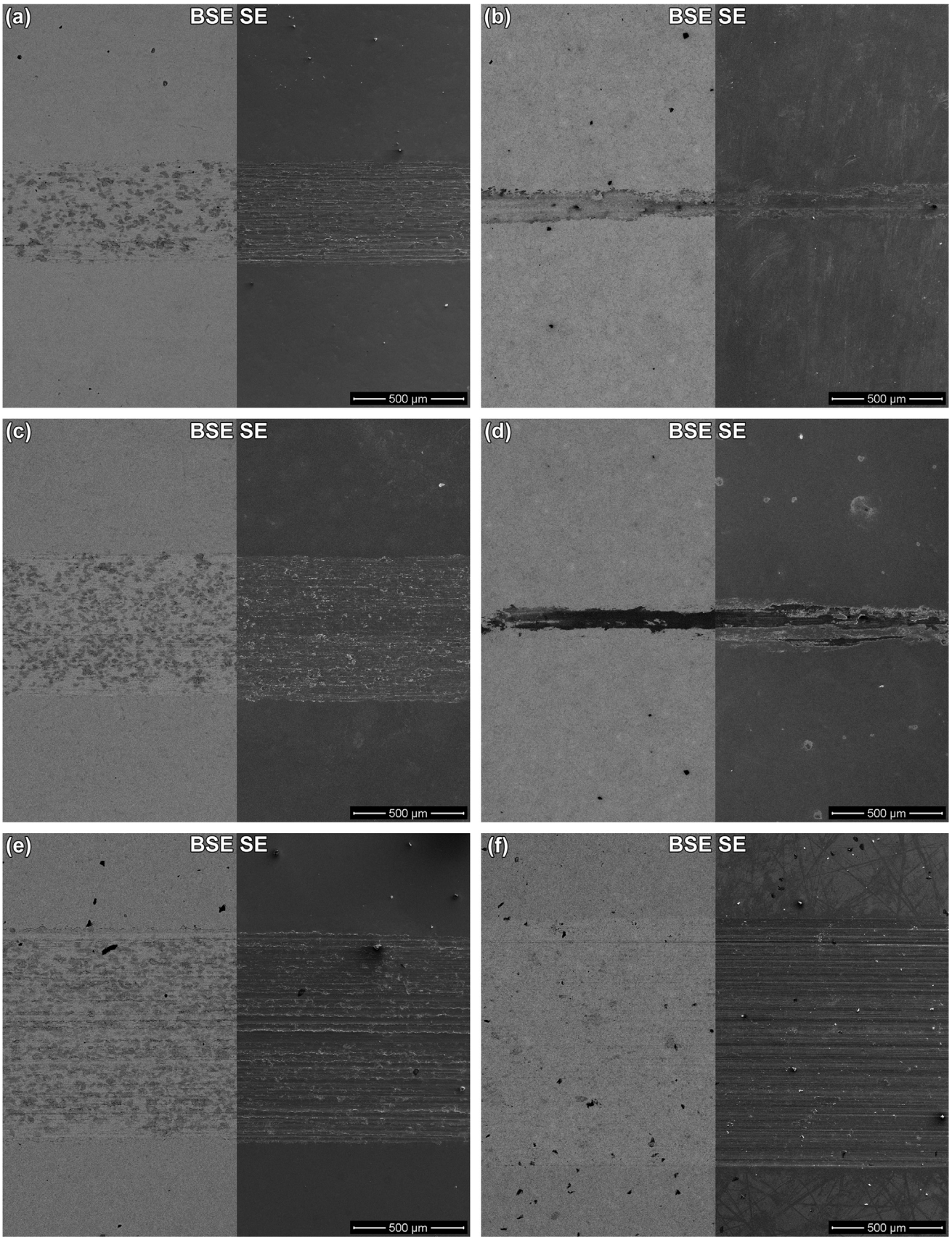

Fig. 5. Low magnification SEM images of the wear tracks of the samples tested under (a,b) 1 N-1 Hz, (c,d) 1 N-2 Hz, and (e,f) 10 N-1 Hz for the unreinforced and composite samples, respectively.

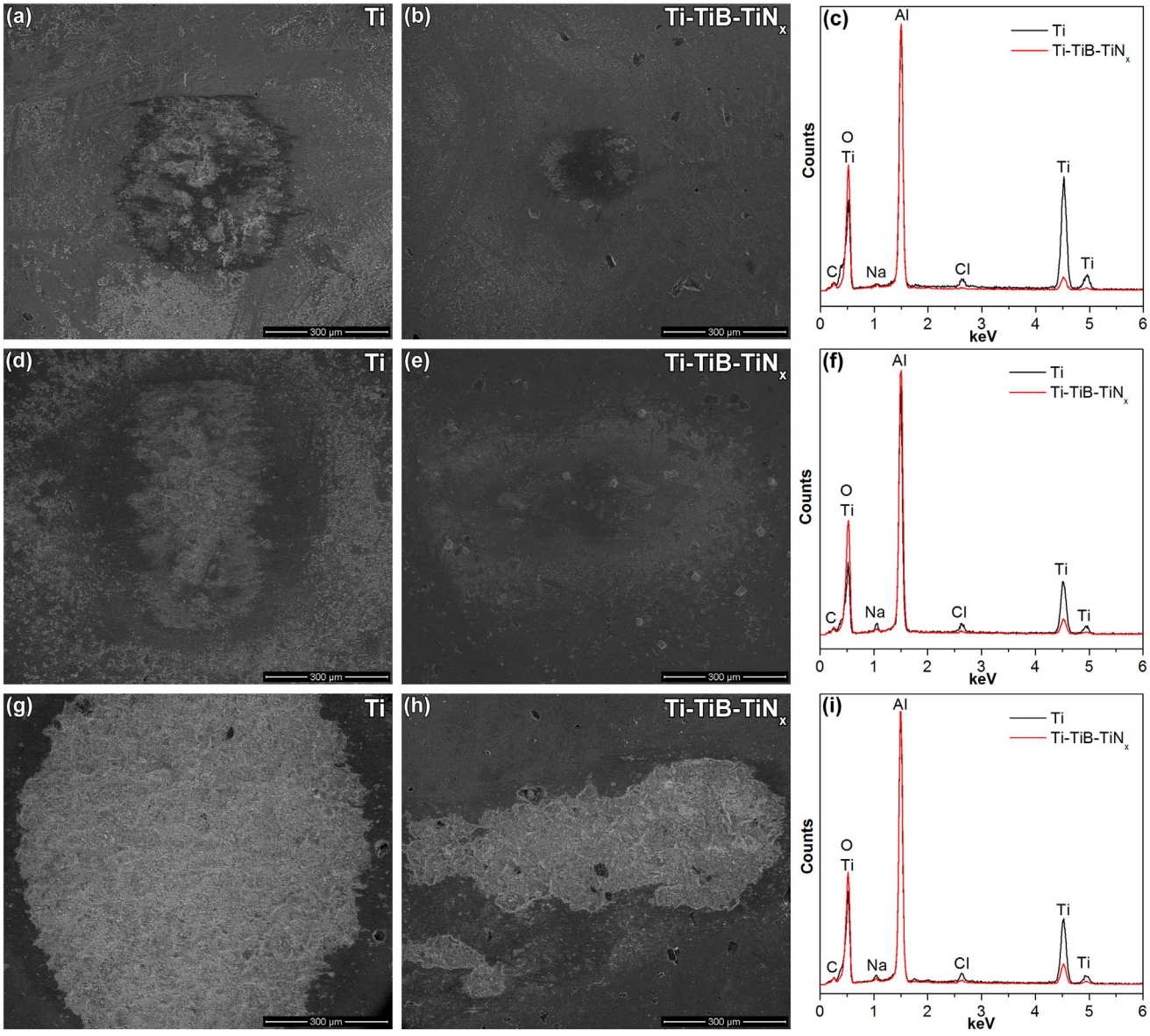

Fig. 6. SE SEM images and EDS spectra of the counter material surfaces worn against unreinforced and composite samples, tested under (a,b,c) 1 N-1 Hz, (d,e,f) 1 N-2 Hz, and (g,h,i) 10 N-1 Hz.

friction (COF) under sliding. Three different zones can be considered on the evolution of the OCP of all samples in all conditions. Before sliding, the OCP values were stable due the presence of a passive film on the sample surfaces in contact with the NaCl solution. When sliding started, except for the composite sample tested under 1 N-1 Hz, a sudden, significant drop on OCP values were recorded indicating an increase on the thermodynamic tendency to corrosion due the mechanical damage of the passive film and the formation of the active zones located in the wear tracks (Ma and Rainforth, 2012; Pina et al., 2015). After sliding, OCP values increased to more positive potential values due to the recovering of the passive film on the worn surfaces.

Regarding the unreinforced material, a similar cathodic shift was observed on the onset of the sliding for all testing conditions where the potential dropped down to the values ranged between −0.65 and −0.72 V. Samples tested under 1 N presented a slight recovery on the OCP values during sliding whereas unreinforced Ti tested under 10 N presented relatively larger oscillations on the OCP values during sliding suggesting more prominent repassivation/depassivation mechanism on the worn surface.

The composite samples tested under 1 N of load and 1 Hz of frequency presented a very small potential drop (approx. 45 mV) at the onset of the sliding however, after a short run-in period (approx. during first 250 s of sliding), the values were increased almost up to the initial values recorded before sliding. When sliding frequency increased, potential drop at the onset of the sliding significantly increased by reaching the values around −0.61 V, but even so, the OCP values under sliding were always higher than the unreinforced Ti tested under the same conditions. In the case of sliding under 10 N, the composite samples exhibited similar potential values as the unreinforced samples.

Evolution of COF is also given in Fig. 4. Regarding the unreinforced samples, as soon as the sliding started, COF values were rapidly reached to the values around 0.4 for all samples. During sliding, COF values of the samples tested under 1 N-1 Hz maintained around the 0.4 during approx. first 1000 s and after this, local increments were observed on the values whereas the other unreinforced samples remained relatively stable till the end of the sliding. Regarding the composite samples, the values first increased up to nearly 0.6 for all conditions, then slightly increased for 1 N-1 Hz, stayed relatively stable with larger oscillations for 1 N-2 Hz, and presented both oscillations and waves for 10 N-1 Hz.

Fig. 5 gives the representative lower magnification SEM images of

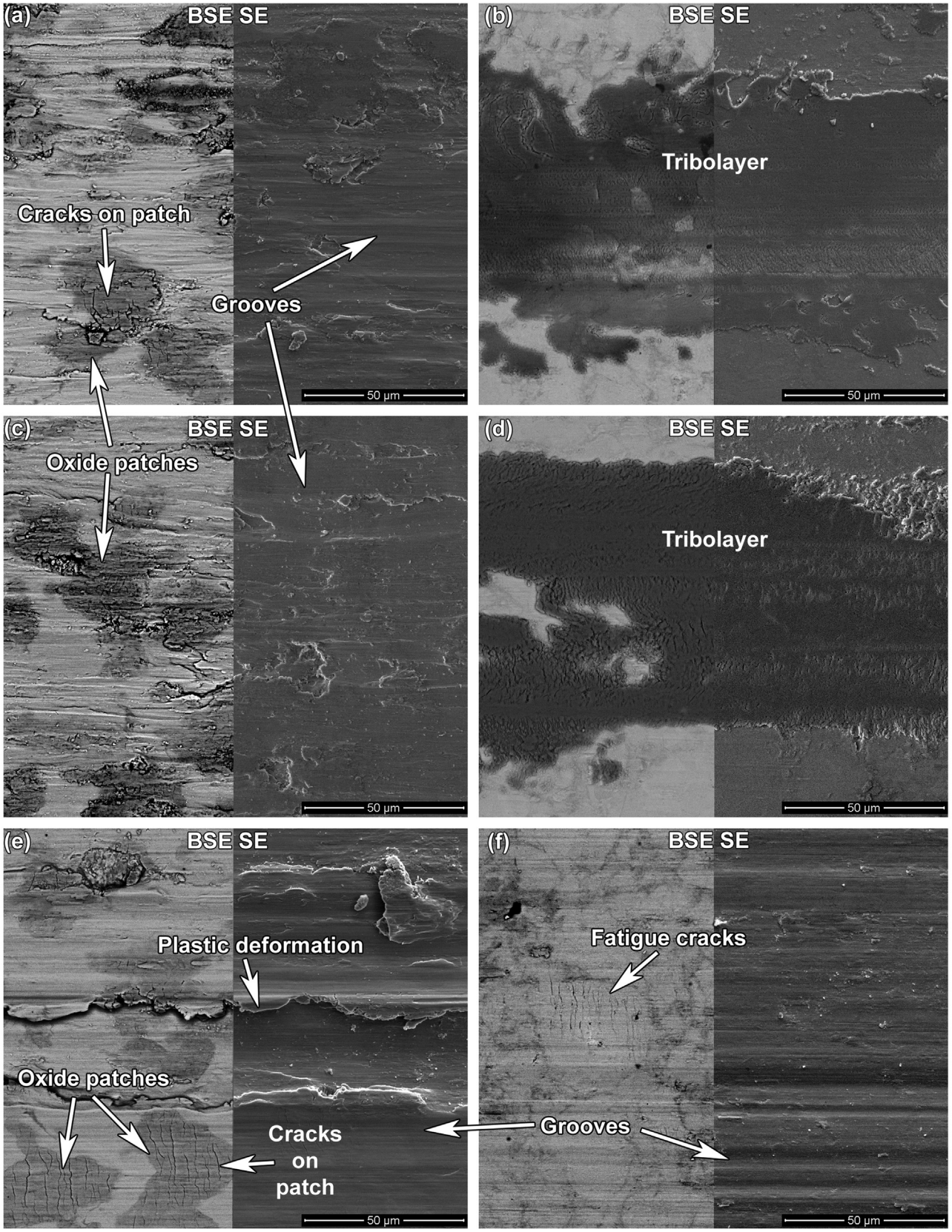

Fig. 7. Higher magnification SEM images of the wear tracks of the samples tested under (a,b) 1 N-1 Hz, (c,d) 1 N-2 Hz, and (d,e) 10 N-1 Hz for the unreinforced and composite samples, respectively.

the wear tracks. Under 1 N, composite samples presented much thinner wear tracks as compared to the unreinforced samples, however, the difference was not significant on the samples tested under 10 N. Tribochemical features, parallel grooves, and abrasion scratches were observed on all worn unreinforced Ti surfaces, presented in BSE and SE modes, respectively. It was also noticed that compacted tribolayers

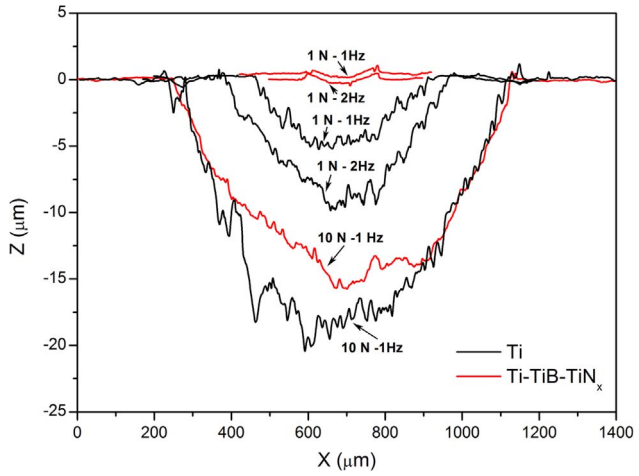

Fig. 8. Wear track profiles.

were formed on the wear tracks of the composite samples tested under 1 N (both for 1 Hz and 2 Hz), however, this was not found on the sample tested under 10 N where parallel sliding grooves and scratches were observed.

Fig. 6 presents the SE SEM images of the worn counter material (Al_2O_3 ball) surfaces and the EDS spectra taken from the wear scars. EDS analysis confirmed material transfer from the samples to the balls for all conditions. The wear scars were relatively larger on the balls slid against the unreinforced samples suggesting an increased action of adhesion. On the other hand, increased frequency or load resulted with larger wear scars for both unreinforced and reinforced samples.

Higher magnification worn surface images (Fig. 7) provides a closer look to the topography and the tribological features. The typical features of adhered/mixed oxide patches for the unreinforced Ti was observed which was formed by repetitive material transfer between the mating surfaces, and meanwhile, oxidation of the entrapped Ti debris on the wear zone (Dong and Bell, 1999; Doni et al., 2013; Yazdanian et al., 2007; Zivic et al., 2011). The effect of these oxides may be twofold; on one hand, they may provide a limited protection by playing a physical barrier role between the sliding surfaces, on the other hand, they can lead to third-body wear by moving freely on the contact zone after fragmentation, thus resulting in formation of abrasion scratches (Quinn, 1983; Srinivasan et al., 2002; Zafari et al., 2012). The oxide patches observed on the Ti samples tested under 1 N were relatively loose whereas Ti samples tested under 10 N presented well-compacted patches, but cracks were observed on the patches in all cases. Additionally, larger sliding grooves and severe plastic deformation was observed on the unreinforced Ti samples tested under 10 N.

Worn composite surfaces, on the other hand, exhibited relatively thick and continuous compacted wear debris layer under 1 N. A compacted wear debris layer was not observed on the worn composite surfaces tested under 10 N, probably due to do higher load that did not allow formation of a compact layer by ejecting the wear debris outside of the wear track, also resulting in more abrasion scratches and sliding grooves. Composite samples tested under 10 N also presented cracks formed perpendicular to the sliding direction (Fig. 7f).

The 2D profiles taken from the wear tracks are given in Fig. 8. It can be seen on the wear profiles that in all conditions, the unreinforced samples presented deeper wear tracks as compared to the Ti−-TiB−TiN_x samples. The total wear volume loss values were given in Table 3. It was observed that as load increased, both Ti and composite samples presented higher wear volume loss. However, while the increase on frequency led to an increase on the total wear volume loss for the unreinforced samples, the difference was not significant on the composite samples.

4. Discussion

In MMCs, apart from corrosion of the matrix metal and degradation of the reinforcement phases, most of the corrosion features are related to the matrix/reinforcement interface, such as galvanic coupling between the matrix and the reinforcement or localized corrosion due to the discontinuities or gaps between the matrix and the reinforcement (Bobic et al., 2009; Hihara and Latanision, 1994; Hu et al., 2004; Otani et al., 1988; Pardo et al., 2005a, 2005b; Ribeiro et al., 2015; Shreir, 1994; Winkler and Flower, 2004; Yue et al., 1999). EIS or potentiodynamic polarization results did not suggest any galvanic coupling between the matrix and the in-situ reinforcing phases. Moreover, since in-situ processing methods offer a 'clean' and physically compatible interfaces, other types of localized corrosion due to the interphases or the gaps at the interface were not observed. It has been reported that ceramic reinforcing phases may act as inert physical barrier thus may increase the corrosion resistance of MMCs as compared to their matrix metal (Feng et al., 2008; Seah et al., 2002). In the composite case, nano-sized in-situ TiN_x phase may contribute to the corrosion resistance by playing an inert physical barrier role on the oxide film resulting with slightly increased R_{ox} values.

Microstructural, chemical, and profilometric analysis of the worn surfaces revealed that incorporation of the reinforcing phases and the sliding parameters significantly influenced the wear and friction behavior. Regarding the COF values, two opposite trends were possible under sliding; (i) COF values tending to decrease due to the formation of the oxide pathes or the tribolayers resulting in decreased metallic area in contact with the counter material; (ii) COF values tending to increase due to the presence of the hard, oxidized wear debris freely moving at the sliding zone resulting in third-body wear (Doni et al., 2013). In the composite case, harder wear debris with the presence of hard ceramic reinforcing phases can further increase the COF values. On the other hand, it has been reported that under higher sliding frequency, thus, higher sliding velocity, it is easier to generate granular debris due to the repetitive tangential stress. The trapped wear debris may act as rolling balls (i.e. solid lubricant) leading to a decrease on the COF values that may also explain the slightly reduced COF values on the samples tested under 1 N-2 Hz as compared to the ones tested under 1 N-1 Hz (Ding et al., 2010, 2009; Zhou et al., 2008). Another interesting observation on the COF values was the local increments recorded for the unreinforced Ti samples tested under 1 N-1 Hz. This behavior may be attributed to the repetitive thickening and breaking of the oxide patches under lower normal load and lower sliding frequency conditions, which may also explain the corresponding local increments on the OCP values where thickening of the oxide patches may provide a limited additional protection against corrosion thus resulted in a slight increment on the corresponding OCP values (Fig. 5).

Table 3
Total wear volume loss values.

	Wear Volume Loss (mm^3)		
Sample	1 N-1 Hz	1 N-2 Hz	10 N-1 Hz
Ti	$(3.21 \pm 1.14) \times 10^{-3}$	$(9.97 \pm 0.62) \times 10^{-3}$	$(3.22 \pm 0.24) \times 10^{-2}$
Ti − TiB − TiNx	$(3.29 \pm 1.29) \times 10^{-5}$	$(2.84 \pm 0.50) \times 10^{-5}$	$(3.01 \pm 0.95) \times 10^{-2}$

The average OCP values were slightly decreased for the unreinforced Ti as the sliding frequency or the load increased, whereas the decrease was more drastic on the composite samples. Berradja et al. (2006) studied the effect of sliding velocity and normal load on the tribocorrosion behavior of stainless steels in a Ringer's solution. The authors reported that when sliding velocity increased, more active material was exposed to the electrolyte for a shorter duration between two contacts. At a given repassivation kinetics, the activation of the surface areas in the wear track during the contact events result in enhancing the dissolution of the material. Thus, lower potential values recorded for the unreinforced and the composite samples tested under 2 Hz can be explained by the increased contact events. It is worthy to point that between 1 N- 1 Hz and 2 N-2 Hz testing conditions, although the cathodic shift on the onset of the sliding was dramatically increased on the composite samples, the total wear volume loss was not significantly different. It is known from the literature that some parameters may influence the material loss due to corrosion, significantly, whereas may not have a significant effect on the total material loss (Runa et al., 2013). Thus, in order to understand the effect of sliding frequency on the material loss due to corrosion or due to mechanical wear, the synergism between corrosion and wear needs to be studied on $Ti-TiB-TiN_x$ composite.

As compared to the samples tested under 1 N, samples tested under 10 N presented different features on the worn surfaces such as severe plastic deformation on the unreinforced samples and wider sliding grooves on the composite samples. The yield strength of commercially pure Ti vary between 165 − 520 MPa (ASTM Handbook – Properties and selection: nonferreous alloys and special propose materials Vol. 2, 1998). The maximum initial Hertzian contact pressure on the unreinforced samples were 0.41 and 0.89 GPa for 1 and 10 N, respectively. Therefore, the severe plastic deformation on the unreinforced samples tested under 10 N can be explained by the contact pressures that exceeded the yield strength of the material. On the other hand, the cracks observed perpendicular to the sliding direction might be generated by fatigue wear. During sliding, a primary crack may originate on the surface at some weak points and may propagate downward along weak planes such as slip planes or dislocation cell boundaries. Moreover, as cracks propagate, fresh surfaces coming in contact with the solution form an oxide film, avoiding the adhesion of these fractures under the influence of the normal load. As sliding continue, a secondary crack can also develop from the primary crack. On the other hand, the primary crack can connect with an existing subsurface crack. When these connected cracks reaches the surface, wear particles can be released (Stachowiak and Batchelor, 2005). Composite samples tested under 10 N, on the other hand, presented much higher wear loss as compared to the samples tested under 1 N probably due to more severe third-body effect, fatigue cracks and lack of tribolayer which apparently provided a protective role. Consequently, higher damage on the surface led to higher activated areas resulted in lower OCP values under sliding. Nevertheless, further studies, especially sub-surface analysis is needed to have a better understanding on the effect of the fatigue wear. As well, further mechanical studies are needed in order to understand the effect of the reinforcing phases on ductility.

Briefly, the dominant wear mechanisms for the unreinforced samples were abrasive and adhesive wear being most notably on the samples tested under higher load and frequency. In addition, oxidative wear also contributed to the wear of the unreinforced samples, whereas severe plastic deformation was observed on the unreinforced samples tested under 10 N. Composite samples tested under 1 N exhibited very small wear loss as compared to the other samples. Although abrasive and adhesive wear features were observed on these samples, the wear behavior was mainly governed by the tribolayer. However, on the absence of the tribolayer, the effect of abrasive and adhesive wear increased on the composite samples tested under 10 N. Besides, fatigue wear was also contributed to the wear of the composite samples tested under 10 N.

Although $Ti-TiB-TiN_x$ composite showed promising behavior within the studied conditions, several studies need to be performed before considering this composite as a biomaterial for load bearing implants. Firstly, a detailed mechanical characterization needs to be done, particularly Young's modulus of the composite should be defined. Tribocorrosion tests should also be studied as a function of critical tribological parameters, especially normal loads corresponding to the ones observed on the load bearing implants. Also, synergism between corrosion and wear needs to be studied by performing tribocorrosion tests on potentiostatic control. Release of metallic ions needs to be quantified both after long-term immersion tests and tribocorrosion tests. The effect of proteins and bio-organisms to the corrosion and tribocorrosion behavior needs to be explored. Finally, the in-vitro and in-vivo biological behavior should be explored.

5. Conclusions

Corrosion and tribocorrosion behavior of the $Ti-TiB-TiN_x$ in-situ hybrid composite synthesized by reactive hot pressing was studied in 9 g/L NaCl solution. Electrochemical studies performed under static conditions suggested that TiB and TiN_x in-situ phases were electrochemically neutral, furthermore, the interface between those reinforcing phases and the Ti matrix did not play a noticeable role on the corrosion behavior. The tribocorrosion behavior of the composite tested under lower normal load was mainly governed by the tribolayer that provided a protective role against tribocorrosion. However, the absence of the protective compact oxide layer under higher load resulted in significantly higher wear damage by abrasion, adhesion, and fatigue wear, as well as higher tendency to corrosion under sliding.

Acknowledgements

This study was supported by The Calouste Gulbenkian Foundation through “Programa de Mobilidade Académica para Professores” and FCT with the reference project UID/EEA/04436/2013, by FEDER funds through the COMPETE 2020 – Programa Operacional Competitividade e Internacionalização (POCI) with the reference project POCI-01-0145-FEDER-006941. F. Toptan is grateful for financial support through the project NORTE 01-0145_FEDER-000018.

References

Aikin, R.M., 1997. The mechanical properties of in-situ composites. JOM 49, 35–39.
Assis, S.L. De, Wolynec, S., Costa, I., 2006. Corrosion characterization of titanium alloys by electrochemical techniques. Electrochim. Acta 51, 1815–1819.
ASTM Handbook, 1998 Properties and Selection: Nonferreous Alloys And Special Propose Materials, Vol. 2, 9th Editio. ed.
Berradja, A., Bratu, F., Benea, L., Willems, G., Celis, J.-P., 2006. Effect of sliding wear on tribocorrosion behaviour of stainless steels in a Ringer's solution. Wear 261, 987–993.
Bobic, B., Mitrovic, S., Babic, M., Bobic, I., 2009. Corrosion of aluminium and zinc-aluminium alloys based metal-matrix composites. Tribol. Ind. 31, 44–53.
Bolzoni, L., Ruiz-Navas, E.M., Neubauer, E., Gordo, E., 2012. Inductive hot-pressing of titanium and titanium alloy powders. Mater. Chem. Phys. 131, 672–679.
Bryant, M., Farrar, R., Freeman, R., Brummitt, K., Nolan, J., Neville, A., 2014. Galvanically enhanced fretting-crevice corrosion of cemented femoral stems. J. Mech. Behav. Biomed. Mater. 40, 275–286.
Chawla, N., Chawla, K.K., 2006. Metal Matrix Composites. Kluwer Academic Publishers, Boston.
Ding, H., Dai, Z., Skuiry, S.C., Hui, D., 2010. Corrosion wear behaviors of micro-arc oxidation coating of Al2O3 on 2024Al in different aqueous environments at fretting contact. Tribol. Int. 43, 868–875.
Ding, H., Zhou, G., Dai, Z., Bu, Y., Jiang, T., 2009. Corrosion wear behaviors of 2024Al in artificial rainwater and seawater at fretting contact. Wear 267, 292–298.
Dong, H., Bell, T., 1999. Tribological behaviour of alumina sliding against Ti6Al4V in unlubricated contact. Wear 225–229, 874–884.
Doni, Z., Alves, A.C., Toptan, F., Gomes, J.R., Ramalho, A., Buciumeanu, M., Palaghian, L., Silva, F.S., 2013. Dry sliding and tribocorrosion behaviour of hot pressed CoCrMo biomedical alloy as compared with the cast CoCrMo and Ti6Al4V alloys. Mater. Des. 52, 47–57.
Doni, Z., Alves, A.C., Toptan, F., Pinto, A.M., Rocha, L.A., Buciumeanu, M., Palaghian, L., Silva, F.S., 2014. Tribocorrosion behaviour of hot pressed CoCrMo − Al_2O_3 composites for biomedical applications. Tribol. - Mater. Surf. Interfaces 8, 201–208.
Feng, Q., Li, T., Teng, H., Zhang, X., Zhang, Y., Liu, C., Jin, J., 2008. Investigation on the

corrosion and oxidation resistance of Ni–Al_2O_3 nano-composite coatings prepared by sediment co-deposition. Surf. Coat. Technol. 202, 4137–4144.
Figueira, N., Silva, T.M., Carmezim, M.J., Fernandes, J.C.S., 2009. Corrosion behaviour of NiTi alloy. Electrochim. Acta 54, 921–926.
González, J.E.G., Mirza-Rosca, J.C., 1999. Study of the corrosion behavior of titanium and some of its alloys for biomedical and dental implant applications. J. Electroanal. Chem. 471, 109–115.
Hihara, L.H., Latanision, R.M., 1994. Corrosion of metal matrix composites. Int. Mater. Rev. 39, 245–264.
Hu, J., Chu, W.Y., Fei, W.D., Zhao, L.C., 2004. Effect of interfacial reaction on corrosion behavior of alumina borate whisker reinforced 6061Al composite. Mater. Sci. Eng. A 374, 153–159.
Li, S., Sun, B., Imai, H., Mimoto, T., Kondoh, K., 2013. Powder metallurgy titanium metal matrix composites reinforced with carbon nanotubes and graphite. Compos. Part A Appl. Sci. Manuf. 48, 57–66.
Licausi, M.P., Igual Muñoz, A., Amigó Borrás, V., 2013. Influence of the fabrication process and fluoride content on the tribocorrosion behaviour of Ti6Al4V biomedical alloy in artificial saliva. J. Mech. Behav. Biomed. Mater. 20, 137–148.
Ma, L., Rainforth, W.M., 2012. The effect of lubrication on the friction and wear of Biolox®delta. Acta Biomater. 8, 2348–2359.
Mathew, M.T., Srinivasa Pai, P., Pourzal, R., Fischer, A., Wimmer, M.A., 2009. Significance of tribocorrosion in biomedical applications: overview and current status. Adv. Tribol. 2009, 1–12.
Mondal, D.P., Das, S., 2006. High stress abrasive wear behaviour of aluminium hard particle composites: effect of experimental parameters, particle size and volume fraction. Tribol. Int. 39, 470–478.
Orazem, M.E., Tribollet, B., 2008. Electrochemical Impedance Spectroscopy. Jonh Wiley & Sons, New Jersey.
Otani, T., McEnaney, B., Scott, V.D., 1988. Corrosion of metal matrix composites. In: Fishman, S.G., Dhingra, A.K. (Eds.), Cast Reinforced Metal Composites. ASM International, pp. 383–390.
Pardo, A., Merino, M.C., Merino, S., Viejo, F., Carboneras, M., Arrabal, R., 2005a. Influence of reinforcement proportion and matrix composition on pitting corrosion behaviour of cast aluminium matrix composites (A3xx.x/SiCp). Corros. Sci. 47, 1750–1764.
Pardo, A., Merino, M.C., Rams, J., Merino, S., Viejo, F., Campo, M., 2005b. Effect of reinforcement coating on the oxidation behavior of AA6061/SiC/20p composite. Oxid. Met. 63, 215–227.
Pina, V.G., Dalmau, A., Devesa, F., Amigó, V., Muñoz, A.I., 2015. Tribocorrosion behavior of beta titanium biomedical alloys in phosphate buffer saline solution. J. Mech. Behav. Biomed. Mater. 46, 59–68.
Quinn, T.F.J., 1983. Review of oxidational wear: part I: the origins of oxidational wear. Tribol. Int. 16, 257–271.
Rahaman, M.N., Yao, A., Bal, B.S., Garino, J.P., Ries, M.D., 2007. Ceramics for prosthetic hip and knee joint replacement. J. Am. Ceram. Soc. 90, 1965–1988.
Ranganath, S., 1997. A review on particulate-reinforced titanium matrix composites. J. Mater. Sci. 32, 1–16.
Rautray, T.R., Narayanan, R., Kim, K.-H., 2011. Ion implantation of titanium based biomaterials. Prog. Mater. Sci. 56, 1137–1177.
Ribeiro, A.M., Alves, A.C., Silva, F.S., Toptan, F., 2015. Electrochemical characterization of hot pressed CoCrMo–HAP biocomposite in a physiological solution. Mater. Corros. 66, 790–795.
Rosso, M., 2006. Ceramic and metal matrix composites: routes and properties. J. Mater. Process. Technol. 175, 364–375.
Runa, M.J., Mathew, M.T., Rocha, L.A., 2013. Tribocorrosion response of the Ti6Al4V alloys commonly used in femoral stems. Tribiol. Int. 68, 85–93.
Sannino, A.P., Rack, H.J., 1995. Dry sliding wear of discontinuously reinforced aluminum composites: review and discussion. Wear 189, 1–19.
Seah, K.H.W., Krishna, M., Vijayalakshmi, V.T., Uchil, J., 2002. Corrosion behaviour of garnet particulate reinforced LM13 Al alloy MMCs. Corros. Sci. 44, 917–925.
Shreir, L., 1994. Corrosion, 3rd ed. 1 Butterworth-Heinemann, London.
Silva, J.I., Alves, A.C., Pinto, A.M., Silva, F.S., Toptan, F., 2016. Dry sliding wear behaviour of Ti-TiB-TiNx in-situ composite synthesised by reactive hot pressing. Int. J. Surf. Sci. Eng. 10, 317–329.
Srinivasan, P.B., Krishnakumar, C.V., Krishnaraj, N., 2002. Sliding wear behavior of salt bath nitrocarburized medium carbon steel. J. Mater. Eng. Perform. 11, 509–515.
Stachowiak, G.W., Batchelor, A.W., 2005. Engineering Tribology. Butterworth Heinemann.
Toptan, F., Alves, A.C., Kerti, I., Ariza, E., Rocha, L.A., 2013. Corrosion and tribocorrosion behaviour of Al-Si-Cu-Mg alloy and its composites reinforced with B4C particles in 0.05M NaCl solution. Wear 306, 27–35.
Toptan, F., Rego, A., Alves, A.C., Guedes, A., 2016. Corrosion and tribocorrosion behavior of Ti–B4C composite intended for orthopaedic implants. J. Mech. Behav. Biomed. Mater. 61, 152–163.
Toptan, F., Rocha, L.A., 2015. Tribocorrosion in metal matrix composites. In: Tyagi, R., Davim, J.P. (Eds.), Processing Techniques and Tribological Behavior of Composite Materials. IGI Global, Hershey PA, pp. 149–167.
Velhinho, A., Botas, J.D., Ariza, E., Gomes, J.R., Rocha, L.A., 2004. Tribocorrosion studies in centrifugally cast Al-matrix SiC p-reinforced functionally graded composites. Mater. Sci. Forum 455–456, 871–875.
Venkataraman, B., Sundararajan, G., 1996. The sliding wear behaviour of Al-SiC particulate composites—I. Macrobehaviour. Acta Mater. 44, 451–460.
Winkler, S.L., Flower, H.M., 2004. Stress corrosion cracking of cast 7XXX aluminium fibre reinforced composites. Corros. Sci. 46, 903–915.
Wood, R.J.K., 2007. Tribo-corrosion of coatings: a review. J. Phys. D. Appl. Phys. 40, 5502–5521.
Yazdanian, M.M., Edrisy, A., Alpas, A.T., 2007. Vacuum sliding behaviour of thermally oxidized Ti–6Al–4V alloy. Surf. Coat. Technol. 202, 1182–1188.
Yue, T.M., Wu, Y.X., Man, H.C., 1999. Improvement in the corrosion resistance of aluminum 2009/SiC w composite by Nd/ YAG laser surface treatment. J. Mater. Sci. Lett. 18, 173–175.
Zafari, A., Ghasemi, H.M., Mahmudi, R., 2012. Tribological behavior of AZ91D magnesium alloy at elevated temperatures. Wear 292–293, 33–40.
Zhou, F., Wang, Y., Ding, H., Wang, M., Yu, M., Dai, Z., 2008. Friction characteristic of micro-arc oxidative Al_2O_3 coatings sliding against Si3N4 balls in various environments. Surf. Coat. Technol. 202, 3808–3814.
Zivic, F., Babic, M., Vencl, A., 2011. Continuous control as alternative route for wear monitoring by measuring penetration depth during linear reciprocating sliding of Ti_6Al_4V alloy. J. Alloy. Compd. 509, 5748–5754.